Localizing Extracellular Vesicles by TREx Microscopy *In Vitro* and *In Vivo*

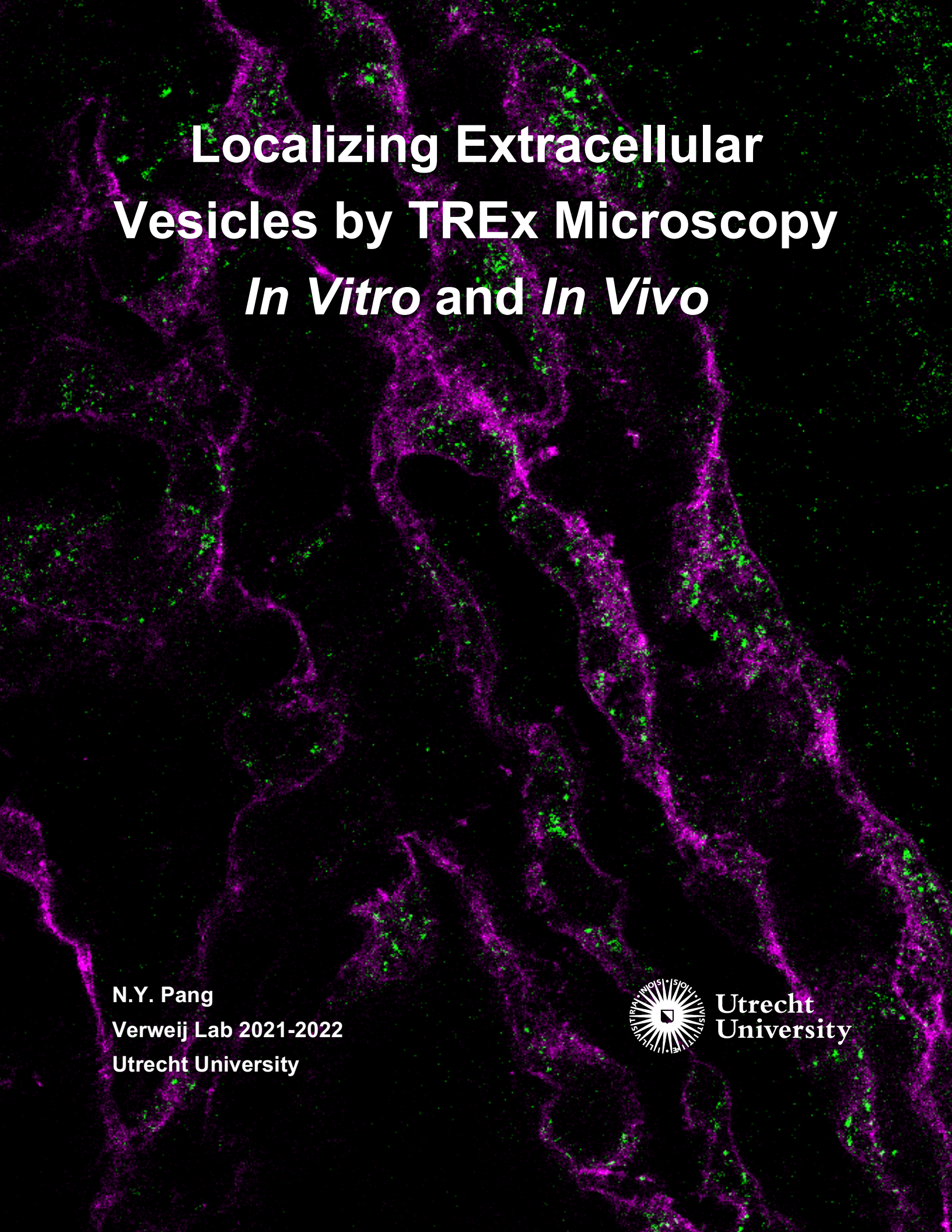

N.Y. Pang
Verweij Lab 2021-2022
Utrecht University

Utrecht University

Table of Contents

Abstract

In this report we present our data for the use of TREx microscopy, an improved expansion microscopy protocol, to visualize extracellular vesicles (EVs) *in vitro* and *in vivo.* Here we focused specifically on exosomes. *In vitro* visualization was done by combining two PM bound MVB markers, ORP1L and Arl8b, with exosome reporter CD63-pHluorin. Here, we found that ORP1L was a better candidate than Arl8b, which caused MVB anomalies. TREx was used to visualize precursor-exosomes, otherwise known as ILVs, with CD63-pHluorin contained in PM bound ORP1L MVBs. Visualization of EVs *in vivo* was was achieved by adaptation and optimization of the TREx protocol for a zebrafish animal model. The main challenges revolved around the optimization of the gel composition to properly embed the fish in the gel and the optimization of expansion kinetics due to tissue heterogeneity which can cause distortions in the sample. Imaging efforts were focused on the caudal vein plexus area of the zebrafish were EVs accumulate. The optimized TREx protocol allowed the visualization of single EVs inside the zebrafish which provided more insight on EV fates *in vivo* with higher resolution than previously acquired. Overall, our research highlights the great potential of TREx microscopy in the field of EVs.

Utrecht University

Sharing science,
shaping tomorrow

Introduction

Extracellular Vesicles (EVs) are small nano-sized lipid bi-layer vesicles secreted by most cells and have long been known to be important vehicles of intercellular communication. Capable of transferring proteins, lipids and nucleic acids, they have the ability to *functionally* influence both recipient and parent cell[1]. They have also been found to be involved in many biological activities such as developmental and homeostatic processes. Besides their roles in physiology, EVs are implicated in various pathologies including cancer progression, which has brought attention to their use as a disease biomarkers and drug nanovehicles[2].

They comprise a heterogeneous population of membrane vesicles that vary in size, density, surface antigens and cargo. According to van Niel[3] they can be subdivided into two main groups, ectosomes and exosomes, which differ in their site of biogenesis. Ectosomes, such as oncosomes and microvesicles are generated at the plasma membrane (PM) by outward budding. Exosomes, by contrast, are produced inside the cell, within the endocytic pathway, by inward budding of the endosomal membrane forming vesicular structures within the endosomal lumen otherwise known as Intraluminal Vesicles (ILVs). These exosome-precursors are contained within multivesicular endosomes or Multivesicular Bodies (MVBs) and may be expelled into the pericellular space upon fusion of these MVBs with the PM. Here, the term MVB is fairly generic and is used to describe various ILV containing compartments or subclasses of early and late endosomes[4]. Although the site of biogenesis serves as a basis for distinction between the groups, these populations still show overlap in terms of composition and size where exosomes range in size of 30-150nm and ectosomes from 50-1000nm[3].

To properly study the fate of these small EVs, a super resolution imaging technique is required to overcome the hurdle of imaging their nanoscale structure. A standard for imaging nanosized samples is Electron Microscopy (EM)[5] but this technique often requires complex sample preparation, professional technicians and can be time consuming[6]. An alternative imaging technique with nano-scale spatial resolution is Expansion microscopy (ExM). It enables super resolution results with normal diffraction-limited microscopes. This technique bypasses the limit by embedding fluorescently labeled specimens in a swellable polymer network followed by is isotropic physical expansion in water resulting in magnification[7] [8]. The improvement in resolution depends on the expansion factor which is 4-fold for the original ExM protocol. Since its first publication, many optimized versions of ExM have been developed[7]. A new variant of this technique called TREx[9] was recently developed in our department with an improved gel recipe that can achieve a 10-fold expansion factor. Although very technical, the general idea of this protocol consists of a few main steps. (1) The sample is fixed, and proteins of interest are fluorescently labeled followed by (2) anchoring of proteins to hydrogel matrix with Acryloyl-X SE (AcX), then the sample is (3) embedded in a monomer solution which is incorporated in the sample during gelation, followed by (4) digestion with proteinase K to mechanically disrupt the sample and finally (5) isotropic expansion in water until the sample is maximally expanded. This technique can also be combined with a grid of fluorescence to validate the expansion of the cells themselves.

For this report we focused on exosomes, the smaller EV subtype. They have long been known to carry functional cargo such as mRNA and miRNAs [10]. The functionality of EVs relies on their ability to function in an autocrine manner, or to interact with local or distant recipient cells in a paracrine or endocrine manner[3] [11]. However, after fusion of the MVBs with the PM and before they can interact with potential recipient cells, the expelled exosomes interact with and navigate the pericellular and extracellular matrix (ECM) where most cells are embedded through their surface associated molecules. For example, proteases and glycosidases on the surface of particular EV subsets play a role in matrix remodeling and degradation[12]. Once they reach a recipient cell, they can either remain bound to the PM, dissociate, directly fuse with the PM and unload their cargo, or be internalized through endocytic pathways where it can also unload its cargo or be degraded in lysosomal compartments[11]. Here, they regulate biological processes through cell signaling cascades initiated by EV-receptor interactions and by different modulatory internalized cargo such as signaling molecules, mRNAs, miRNAs and lipids[12,13]. Moreover, this cell-cell communication can also be cell-type specific when exosomes interact with recipient cells through specific receptor-ligand interactions[10]. These features have also related to pathological processes. Studies in cancer have shown[14] how important intercellular communication is for metastatic progression. It was found that carcinoma derived EVs promote metastatic growth by inducing the formation of pre-metastatic niches when these EVs were taken up by. Although cargo transfer to the recipient cell plays a significant role, it is worth noting that it might not be the main function of EV secretion and that there are still important questions to be answered surrounding other EV functions such as recipient cell surface signaling, trophic support, clearance of obsolete cellular material and modulation of interstitial fluid or extracellular matrix[3]. Furthermore, there are still knowledge gaps surrounding EV transit *in vivo* and the mechanisms of cargo delivery for functional use[3]. Although there has been a lot of progress in the field of EVs, most studies so far have relied on isolation of EVs from biofluids or *in vitro* cell culture supernatant which lacks information on dynamics of EV release, biodistribution, and other contributions to pathophysiology mainly due to the challenges associated with imaging EVs at the single vesicle level[2].

One of these challenges include the study of EV formation in the cell before they are expelled. Before these structures can be resolved they must first be identified. A commonly used reporter for exosomes is tetraspanin protein CD63 which can be localized on the cell surface and in the endosomal system where it is especially enriched in late endosomes on ILVs. However, the specificity is reduced since it can also be found abundantly on lysosomes and other Lysosome Related Organelles[15]. Moreover, exosomes are generated from ILV containing MVBs that travel towards and fuse with the PM but these MVBs can also fuse with lysosomes where they are fated presumably for degradation[4]. Localization then requires a reporter that can specifically identify MVBs bound for fusion with the PM.

One issue is that the exact underlying molecular mechanisms of these secretory MVBs are not well understood. Interestingly, recent work in our lab has shed light on some aspects of exosome secretion[4]. Endosomal compartments at the pre-lysosomal stage undergo a multistep process regulated by GTPases and the endoplasmic reticulum (ER) that affect its ability to fuse with the PM. MVBs bound for the PM undergo a cascade like GTPase identity progression from Rab7a to Arl8b to Rab27a. In this step like progression, small GTPase Arl8b is switched with Rab7 to recruit Rab27 which can be found on fusion competent MVBs. Knockdown of Arl8b reduced exosome

secretion by a fourfold factor[4], further highlighting its important role in this process. ORP1L interacts with Rab7 which can be found on late endocytic compartments[16] and also plays a dynamic role with the ER through the formation of membrane contact sites (MCS) that affect MVB motility, maturation and GTPase identity. In this highly dynamic pathway MVBs can either be tethered or unbound to the ER via MCSs by cholesterol sensing protein ORP1L[17]. This protein makes contact sites with the ER by binding to ER-resident protein VAP-A; this simultaneously inhibits minus end transport which affects MVB progression. Variants ORP1L-dORD and ORP1L-dORDPHDPHD of this protein respectively stimulate ER/MVB MCS formation or recruit MVBs to the perinuclear region. ORP1L-dORDPHDPHD stimulates fusion activity, likely by promoting the Rab7/Arl8b switch. This suggests that ILVs could be more easily visible with the ORP1L-dORDPHDPHD variant. Arl8b and ORP1L can be used in combination with exosome marker CD63 to specifically localize late ILVs inside MVBs destined for the PM in the cell.

Although these reporters work well *in vitro*, it can prove challenging to use them *in vivo*. Fortunately, an *in vivo* model has recently been developed in zebrafish embryos capable of studying EV function with high accuracy [18]. Zebrafish are an excellent model organism for tracking EVs because of their small size, making them relatively easy to work with, their transparency at the embryonic and larval stage useful for light microscopy and they represent a vertebrate system with relevant homology with humans. Moreover, they also possess a stereotyped vasculature and maturating immune system making them ideal to visualize EVs circulating in the body[19]. This *in vivo* model makes use of CD63-pHluorin, a fluorescent CD63 protein reporter which is injected directly in the Yolk Syncytial Layer (YSL) of zebrafish embryos at the 1000 cell stage where they are expressed and released into the blood flow and can be found in different parts of the vasculature. The secreted EVs especially accumulate in the Caudal Vein Plexus (CVP) area where they are either captured, endocytosed or degraded.

For this project we attempt to enable addressing the knowledge gaps by visualizing EVs with TREx to overcome the resolution challenges of imaging EV. Here we performed TREx without any major changes *in vitro* on single cells and implemented an adapted version of TREx *in vivo* on zebrafish embryos. Overall, describe the challenges of this protocol and how it can be used visualize EVs.

Results

EV localization *in vitro*

TREx a powerful imaging technique capable of overcoming the diffraction limit and resolving ultrastructural features without the need of specialized equipment and procedures[9], meaning we can apply standard labeling methods to visualize proteins of interest. Since EVs are nanoscale structures that are difficult to observe with normal imaging techniques we decided to investigate EVs with TREx, however, there are some things we need to keep in mind with this technique. Post-acquisition analysis of TREx specimens can be hard to process if the subcellular structure we wish to observe is not abundantly present or the signal bright enough. Moreover, it is generally better if the cellular target of interest is well labeled since signal intensity of the specimen is reduced due the physical expansion. This can make it very challenging to localize ILVs or future exosomes inside MVBs bound for the PM without a proper biological marker. Therefore, it is important to identify the right marker for our subcellular structure or compartment of interest. We intend to utilize the well-established exosome labeling agent CD63 for our experiments. However, this labeling agent might be overly abundantly present inside the cell which makes analysis and distinction of features post-acquisition quite difficult. To aid this effort we combined CD63 with labeling agents for MVBs. Recent work in our lab has shown that Arl8b and ORP1L are potential marker candidates for PM bound MVBs, a prerequisite for exosome release. However, we need to determine which one works best. Therefore, we labeled cells using variants of small GTPase Arl8b and ORP1L in combination with CD63, compared the results, and chose the best one to proceed with expansion.

Arl8b interaction with CD63

To label PM bound MVBs, three different variants of Arl8b were used. We utilized a wildtype variant (WT) and 2 mutants, constitutively active (CA) and dominant negative (DN), in combination with CD63-pHmScarlett. Here all GTPase variants were tagged with GFP fluorophore. In its native state, Arl8b switches from active to inactive depending if its GTP-bound or GDP-bound respectively[20]. Overexpression of GTP-bound wildtype variant Arl8b-wt-GFP is known to double MVB-PM fusion activity[4]. The CA mutant Arl8b-Q75L remains in the active state since it is deficient in GTP hydrolysis and promotes fusion activity similar to WT. The DN mutant Arl8b-T34N remains in the inactive state since the guanine nucleotide exchange factors are blocked and is known to reduce fusion activity by 2.5 fold [4,20]. We expressed Arl8b variants with CD63 and found that transfected Arl8b variants appeared brighter than the CD63-pHmScarlet, so we transfected less Arl8b compared to CD63. We found that the WT and CA variants had similar expression with the CA sometimes being more abundant which was expected (Fig. 1A). In these two we see that Arl8b localizes to the CD63-pHmScarlet positive endosomes and could be seen by rings around the endosomal structures (Fig. 1B). The dominant negative variant is more homogeneously distributed throughout the cytosol except for some very prominent small rings that are located throughout the cell but can often be seen at the periphery of the cell (Fig. 1A). Although Arl8b might be an option to localize MVBs, the wildtype and active variant expression was often

abundantly present making distinction between single MVBs challenging. Moreover, Arl8b could also be seen expressed without colocalizing with CD63-pHmScarlet positive endosomal bodies (Fig. 1B). Furthermore, we could observe many unusually large endosomal rings which were not present when we only express CD63-pHmScarlet (data not shown). This indicates that the overexpression of Arl8b might be affecting the progression of the endosomal bodies (Fig. 1B). Taking all these actors into account, we concluded that Arl8b might not be the most suitable marker for our purposes.

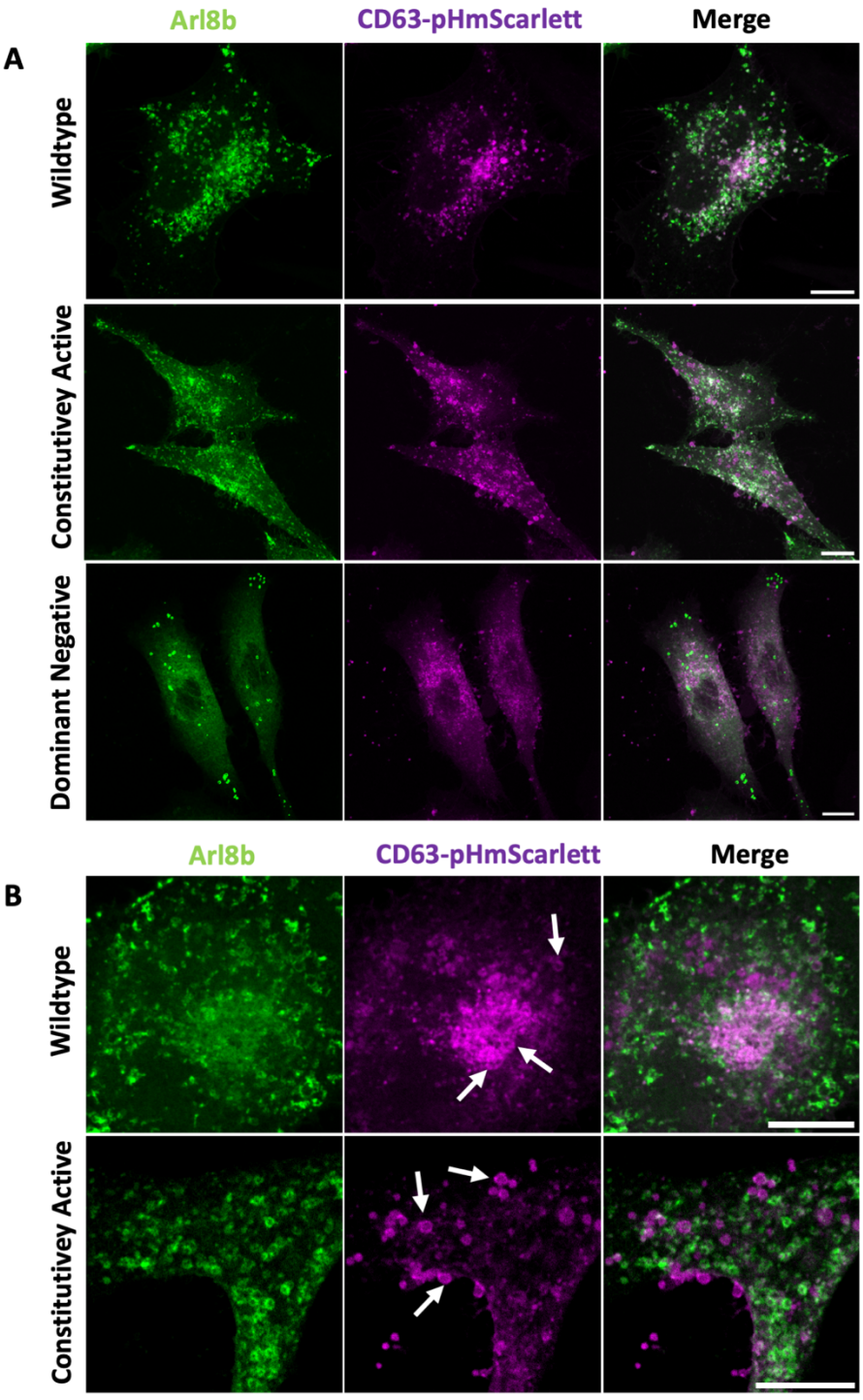

Figure 1 | **GTPase Arl8b variants with endosomal CD63**. **(A)** Confocal light microscopy distribution analysis of different variants of Arl8b-GFP with CD63-pHmScarlett in Hela cells. Arl8b variants include wildtype, Q75L (Constitutively Active) and T34N (Dominant Negative). **(B)** This image shows a close-up of the CA and wildtype variants of Arl8b. The same columns as figure 1A apply here. These variants were also expressed with CD63-pHmScarlet in HeLa cells. The first column shows the presence of many Arl8b rings while the second column displays many abnormally large endosomal ring structures indicated by arrows. The scale bars all indicate 10 μm.

ORP1L interaction with CD63

An alternative method for locating MVBs is by looking at the interaction between CD63 and ORP1L variants. Exosome protein CD63 colocalizes strongly with Rab7[4] and ORP1L functions as an effector to Rab7 found on MVBs. We use this property to localize MVBs. We had three options to choose from, the wildtype and two mutants, ORP1L-dORD and ORP1L-dORDPHDPHD. We expressed the variants with CD63-pHmScarlet, however, only data from the ORP1L-dORD variant was collected. In accordance with literature[21], the ORP1L protein could be found recruited onto the surface of CD63-pHmScarlet positive compartments. We found that it formed clear rings around endosomal compartments (Fig. 2A) with the majority surrounding endosomal compartments, not isolated in the cytoplasm, unlike Arl8b. Furthermore, there were also some endosomal rings found (Fig. 2B), but these were lower in number and size compared to Arl8b. Interestingly some of these rings could be seen around DAPI labeled structures (Fig. 2B). Overall, this option appeared to give a much clearer representation of MVBs compared to the Arl8b variants, showing that they are better candidates for expansion microscopy.

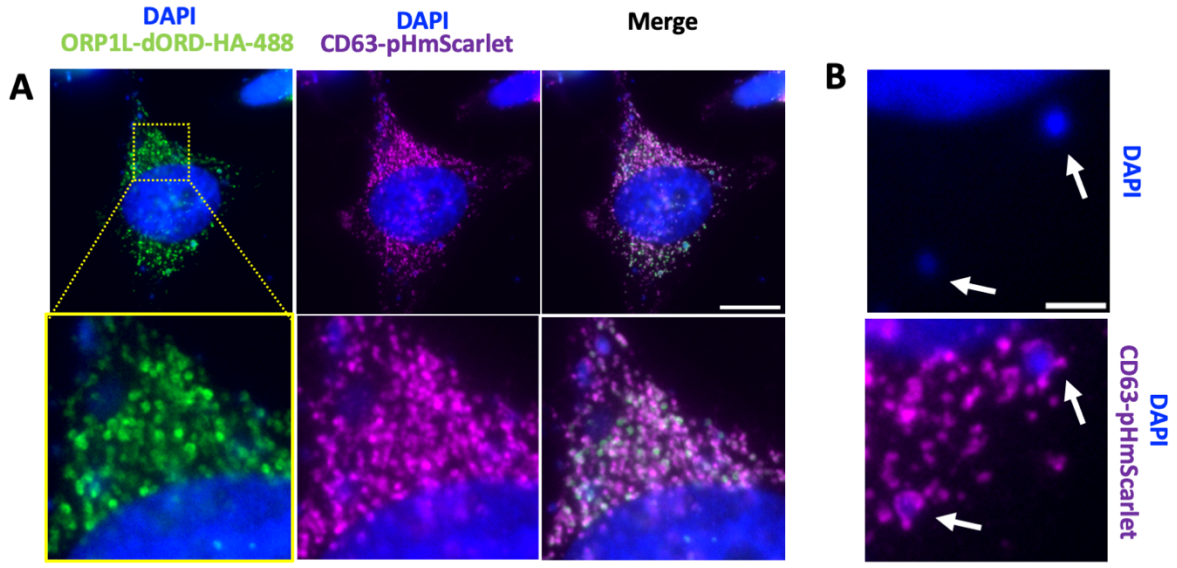

Figure 2 | **ORP1L as an MVB marker with endosomal CD63. (A)** Different channels of HeLa cells expression of ORP1L-dORD-HA-488 with CD63pHmScarlet. Scale bar indicates 10 μm **(B)** Arrows indicate DAPI structures with endosomal rings around them. Scale bar indicates 2 μm.

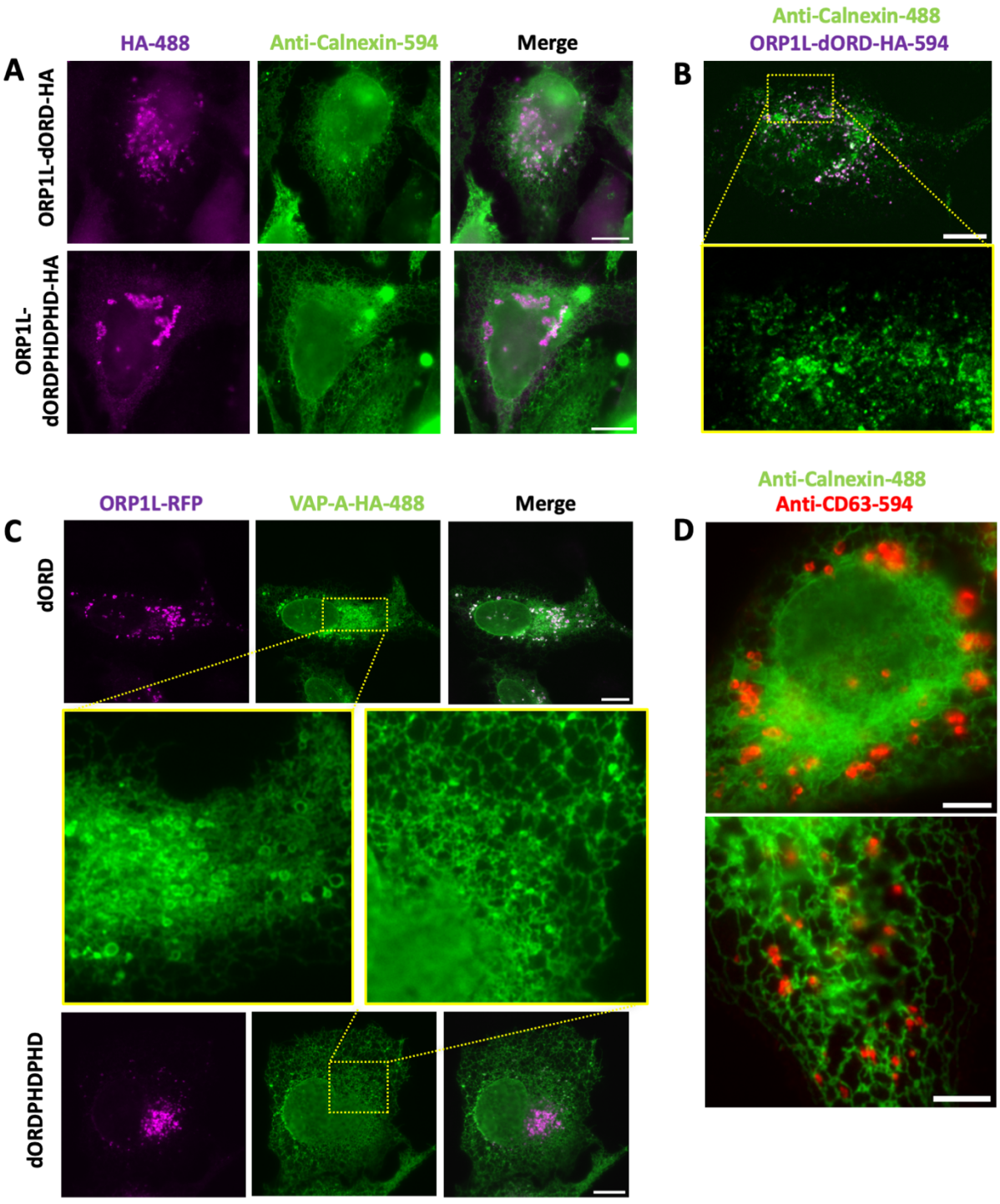

Figure 3 | **ORP1L, ER and endosomal CD63 interaction. (A)** Anti-Calnexin-594 labeling on Hela cells for ORP1L variants with HA tag (colors are adapted to match the rest). Dotty staining of Calnexin was resolved here by adding sucrose and glutaraldehyde in fixation method. **(B)** Dotty staining of anti-calnexin on HeLa cells. **(C)** Overexpression of VAP-A-HA-488 and ORP1L variants ORP1L-dORD-RFP and ORP1L-dORDPHDPHD-RFP on U2OS cells. **(D)** Endogenous immunolabeling of endosomes with anti-CD63-594 and ER with anti-Calnexin-488. Image shows how endosomal bodies interact with the ER. The scale bars in all images indicate 10 µm except for figure D which is 5 µm for both images.

ORP1L interaction with ER

As previously mentioned, the two ORP1L mutants affect endosomal motility and interaction with the ER by forming MCS. Both the progression stage of MVBs and MCS interactions between the ER and MVBs might impact ILV formation. To shed light on possible ILV differences, we first validated the phenotype of both mutants. For this we used ER protein Calnexin and VAP-A protein. We first immunolabeled endogenous calnexin with transfected ORP1L plasmids and found the expected distribution of the dORD variant to be scattered throughout the cell and the dORDPHDPHD variant to be located around the nuclear periphery (Fig. 3A). This distribution result of the ORP1L variants was consistent with previous literature[4,17]. At first, we found that it was difficult to label the calnexin protein since the expression was appearing very dotty (Fig. 3B). This issue was later resolved after changing the fixation method by adding Glutaraldehyde and Sucrose. Since the calnexin staining was very dotty, expansion would only exaggerate this effect and lower the signal even more. To compensate for this, we labeled the ER with VAP-A protein with an HA tag which is a better candidate for ER/LE MCS since this VAP-A makes direct contact with the ORP1L[21]. With the HA tag now being used for the ER instead of ORP1L we switched to RFP tagged ORP1L variants. This combination resulted in very clear ER rings wrapped around MVBs for the dORD variants (Fig. 3C). The dORDPHDPHD variant also showed ER rings but these were not as pronounced as dORD. Additionally, VAP-A displayed a brighter signal intensity compared to calnexin. Expansion microscopy reduces the fluorescent protein signal intensity due to the physical expansion. Therefore, even though both ER proteins showed the same expected distribution in combination with ORP1L (Fig. 3, A and C), VAP-A was the more favorable choice for expansion microscopy.

We also immunolabeled both endogenous Calnexin and CD63 without any ORP1L variants (Fig. 3D) to get an impression of the ER and endosomal distribution under normal circumstances without overexpression. We found that the endosomes were in close proximity to the ER membrane and were scattered throughout the entire cell but that the ER did not have pronounced ring formations here. Endosomal rings could also be seen here but there were no unusually large rings as was the case with the Arl8b overexpression. We found that the results were very useful to compare against the ORP1L variants distribution (Fig. 3, A and C) further validating the expected interaction of the ORP1L with the ER.

After comparing all the discovered results for both MVB markers, Arl8b and ORP1L, we concluded that the ORP1L marker was the better choice for an MVB marker. Ultimately, the main reasons were that ORP1L as a marker showed no significant endosomal anomalies and the MVBs were also clearly distinguishable which wasn't the case with Arl8b. Additionally, by using this marker we can get more detail on MVB motility due to MCS. Altogether this made ORP1L the more appropriate choice for our research needs.

Resolving MVB ultrastructures with TREx combined with ORP1L labelling

Since ORP1L labeling seemed most promising we proceeded with expansion with this MVB marker. We added general protein staining dye maleimide, a bright staining agent which labels thiol biomolecules to see more subcellular details and expanded the specimens using TREx microscopy. This dye clearly revealed that the MVBs were not empty but contained what appeared to be ILVs. This could be seen by dense labeling inside the MVBs in the form of circular structures (Fig. 4A). To show that the circular structures are ILVs we added the CD63-pHluorin reporter. During this process we saw that ILVs were not always clearly visible. This could be the result of our detergent Triton-X causing too much membrane disruption. Therefore, we sought to use a lighter detergent, Saponin, prior to labeling the cells. However, this did not make any significant improvements on the clarity of ILVs and circular structures could also not be seen with the CD63 reporter (Fig. 4B). Therefore, we continued with the previous detergent Triton X-100 and we selected the images with the clearest results. Here, we did find circular structures inside MVBs for the CD63 reporter, indicating that these are indeed ILVs (Fig. 5). Moreover, we found that ORP1L-dORDPHDPHD variants seemed to have denser ILV labeling (Fig. 5B) inside the organelle and a slightly smaller size compared to ORP1L-dORD variants (Fig. 5A). Having successfully used TREx to label ILVs inside MVBs on single cells in culture, we moved expansion study on zebrafish embryo specimens.

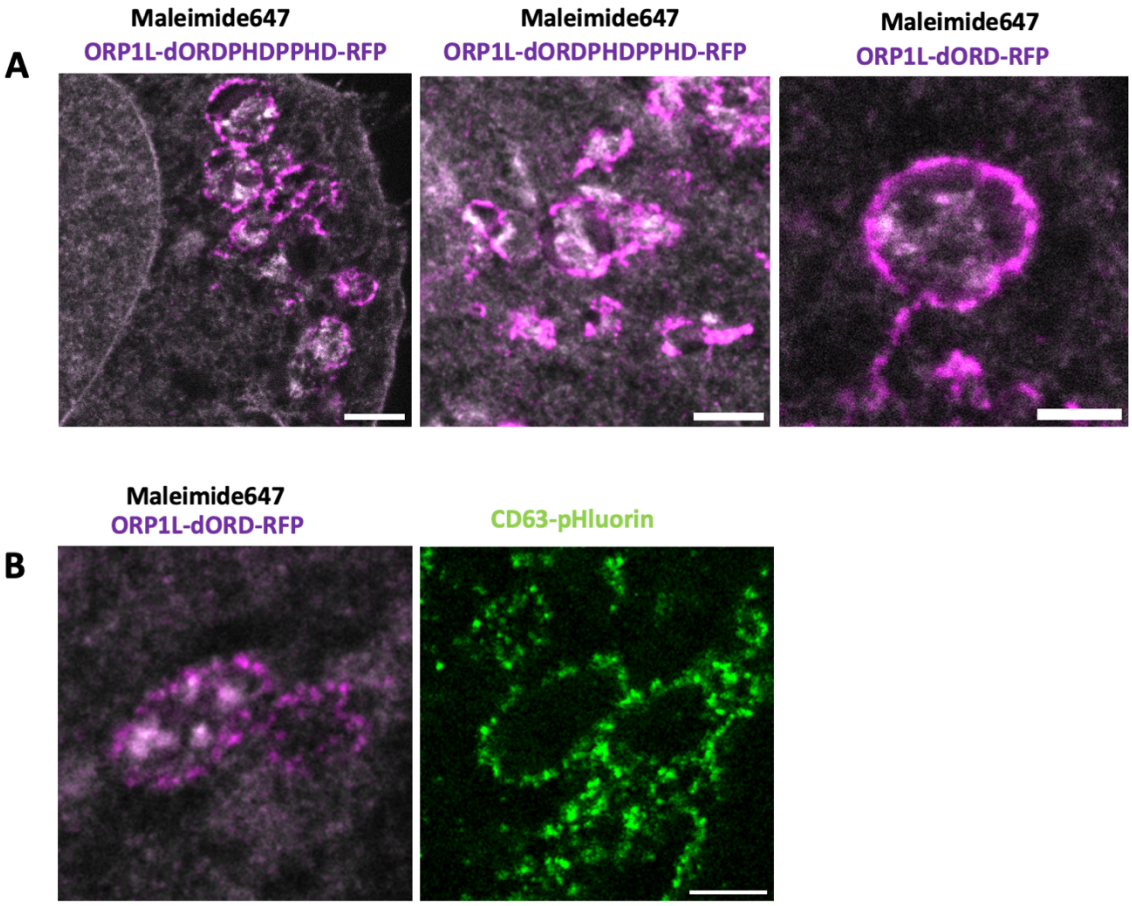

Figure 4 | **TREx microscopy of ORP1L mutants along with maleimide total protein staining showing content inside MVB on HeLa cells. (A)** Various MVBs could be seen with content inside in the form of circular structures, most likely ILVs, labeled by total protein staining Maleimide647. Clusters of ORP1L-dORDPHDPHD MVBs can be seen on the left and middle images. Scale bar indicates 1 μm for both. The right image shows ORP1L-dORD which also contains what appears to be ILVs. Scale bar indicates 500nm. **(B)** Here, detergent Saponin is used as a softer permeabilization agent. The left image shows the dORD variant with MVB contents but with no significant increase in clarity compared to permeabilization agent Triton X-100. Right image shows the same MVB for the CD63 channel but no ILVs could be seen inside. Scale bar indicates 1 μm.

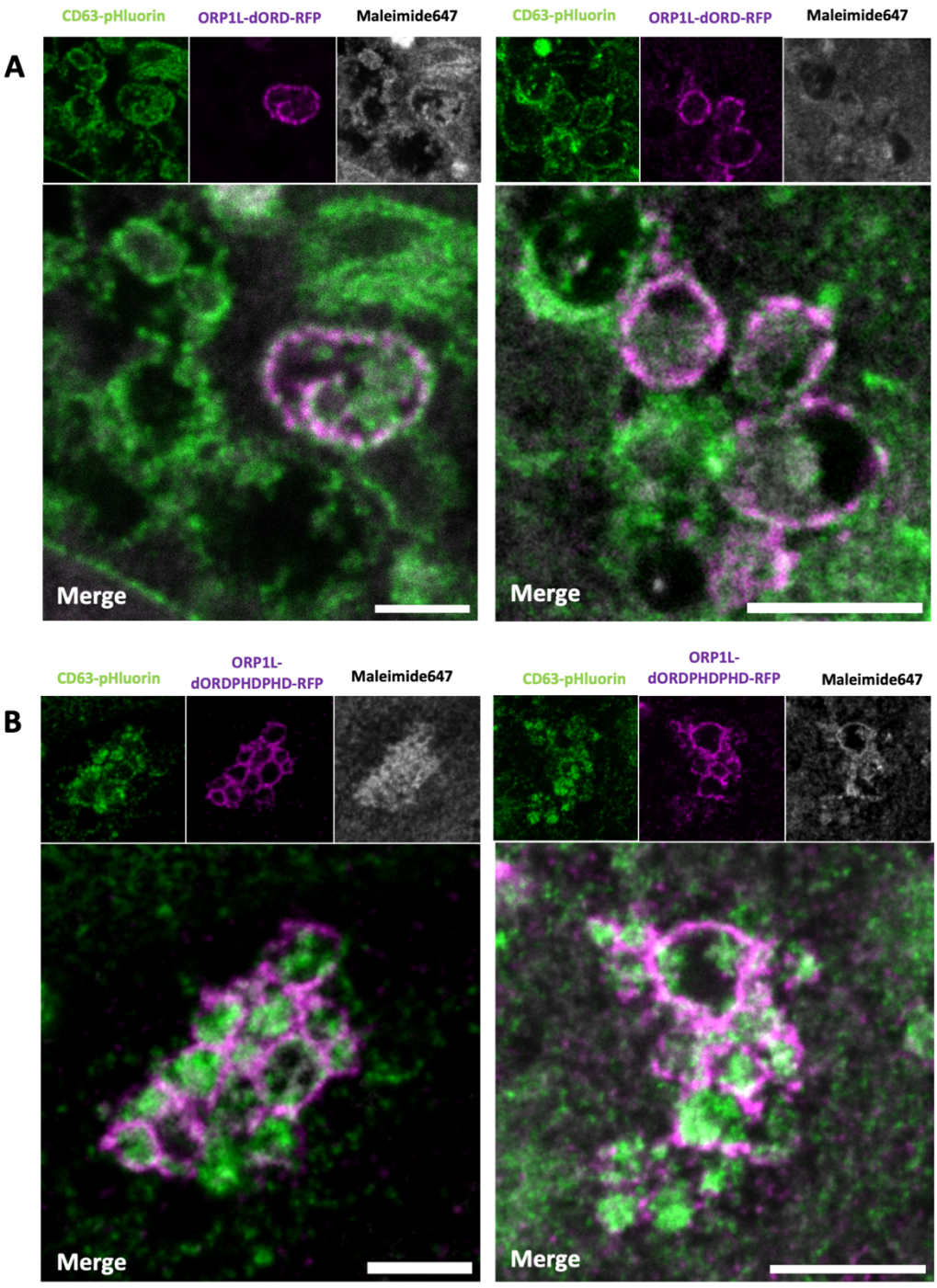

Figure 5 | **TREx microscopy of ORP1L mutants with CD63-pHluorin reporter reveals ILVs inside MVBs (A) &** (**B**) The top 3 images show CD63-pHluorin, ORP1L-RFP variant & maleimide647 respectively and the bottom shows a merge of the isolated channels. **(A)** The ORP1L-dORD variant can be seen with clear ILV structures labeled by the CD63-pHluorin reporter. **(B)** The ORP1L-dORDPHDPHD variant is seen clustered together with clear ILV structures inside. All scale bars indicate 1 μm.

EV localization *in vivo*

Zebrafish Expansion

Previously, our lab[18] developed an animal model where EVs can be tracked *in vivo* by expressing CD63-pHluorin in zebrafish embryos. This was combined with fluorescent labeling of the zebrafish vasculature to study EV function, and it was found that EVs accumulate at the Caudal Vein Plexus (CVP). However, due to resolution constraints, it remained difficult to assess if these EVs remain tethered at the surface or are taken up inside the cell by fusion or endocytosis. To overcome this challenge, we combined this animal model with TREx microscopy.

Before we could image the CVP area we first needed to properly expand the zebrafish with the TREx protocol. For straightforward assessment of general tissue integrity after expansion, we first labeled the fish with DAPI and with a far-red general protein staining dye called maleimide and proceeded with expansion 3-6 days post fertilization old larvae. Additionally, the dye we used had super bright expression which is useful for expansion microscopy. This labeling step was performed identical to the one on single cells and was done in PBS. We found that this step already caused the gels to expand 2X. The dye was washed off and we proceeded with the digestion and expansion steps. The first experiment resulted in an expansion factor of 3.5X (Fig. 6A). Even with the 20X objective this already increased the resolution where we could see fine details of muscle cells and filament like structures (Fig. 6A). However, we found that the overall structural integrity of the fish was compromised, judged from the presence of muscle cells in the yolk region that do not belong there, as well as large gaps, void of any labelling.

The disorganized internal features could be result of several issues such as the gel monomer composition, monomer perfusion through the fish and/or gelation. Initially, we changed our embedding method by reducing the amount of gel polymerization inhibitor 4HT (4-hydroxy-TEMPO). We also increased the gel monomer incubation and gelation time and found that this seemed to help somewhat with embedding the fish inside the gel. Features inside the fish now seemed less disorganized but large gaps could still be observed (Fig. 6, B and D). Taking a higher magnification of 60X showed some of the detail that could be acquired (Fig. 6C). However, the larvae still lacked some structural integrity. We knew this was a problem because it could be seen how cells in expanded samples were flowing out of the zebrafish body during live acquisition (data not shown).

We then acquired images of DAPI & maleimide labeled zebrafish pre-expansion to compare to the same fish after expansion (Fig. 6E). Some fish were cut in half to make the sample smaller, reduce imaging time and facilitate perfusion of the gel monomer solution through the larvae. We found that at the pre-expansion stage, muscles tissue was tightly packed together, and other features of the fish had more clear distinctions and borders but there were also already some cracks that could be seen (Fig. 6E). These cracks only worsened after expansion as could previously be seen by the large gaps in the fish (Fig. 6, B and D).

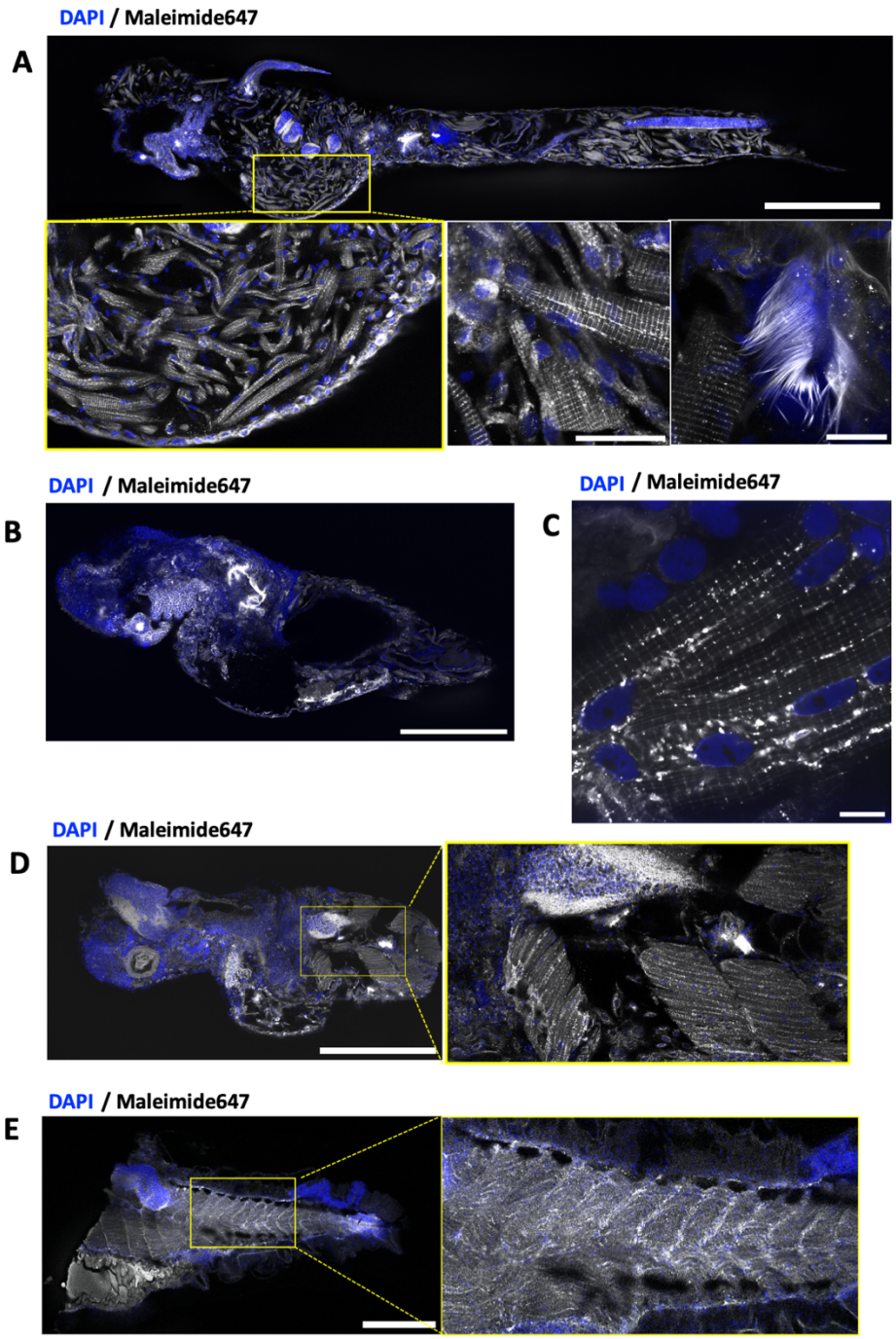

Figure 6 | **Quality and structural integrity of TREx on Zebrafish with DAPI and maleimide total protein staining** **(A)** 3.5-fold expanded zebrafish imaged with 20X air objective, scale bar 2 mm. The bottom images show some highlights of the fish above. The zoomed section shows a portion of the belly with disorganized features, muscles that don't belong there can be seen. Bottom middle image shows a closer view of some muscle cells, scale bar indicates 50 µm. Bottom right image highlights the increase in resolution by the very fine structures that can be seen. (**B)** Anterior half of zebrafish, after embedding was optimized fish features were less disorganized. Scale bar indicates 500 µm. **(C)** Closer up example of fine structures and fibers of muscle cells visible with 60X objective. Scale bar indicates 10 µm. (**D)** Post-Expansion image showing large gaps missing, zoom section of right highlights the gaps. Scale bar indicates 500 µm. (**E)** Pre-expanded tail of zebrafish with muscles tightly packed, zoom section shows there are already cracks forming at connective tissue due to the maleimide labeling step. Scale bar indicates 500 µm.

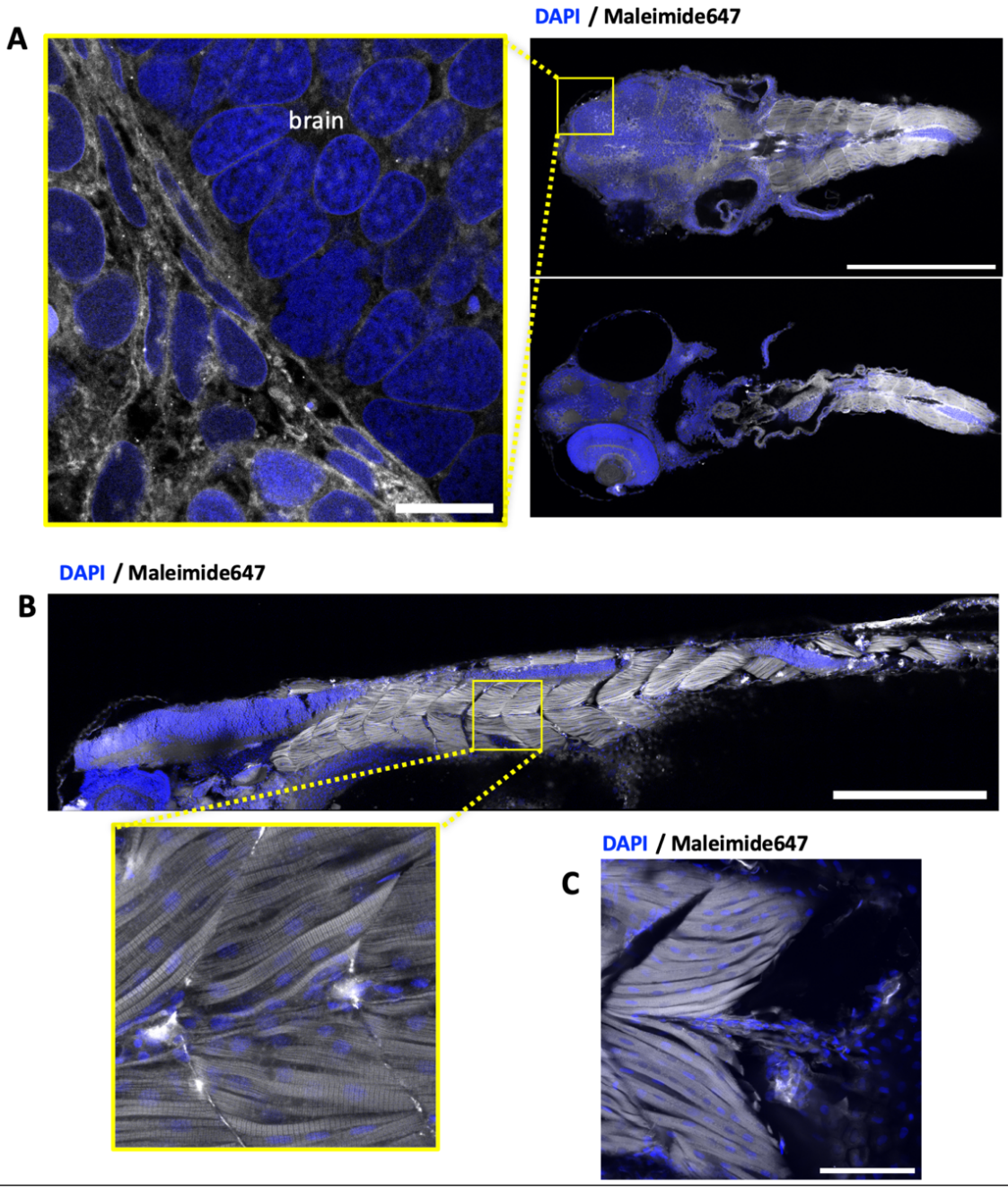

Figure 7 | **Post-digestion maleimide labeling and serial salt decrease improves TREx quality on zebrafish (A)** Left image shows a close-up portion of the zebrafish brain where different cell tissue types intersect. Scale bar indicates 10 µm. Top right image shows a cross-section of the zebrafish along head and midbody region. Right bottom shows the same fish at a lower plane. In both cases muscles are tightly packed and no significant distortions can be seen. Scalebar indicates 500 µm. (**B)** TREx was performed on the fish with pre-digestion maleimide labeling and the expansion was done serially by decreasing the salt concentration gradually. Bottom left zoom image shows how the distortions are reduced by the serial salt decrease step. The tail region, however, did not expand properly. Scale bar indicates 500 µm. **(C)** Example of different sample with pre-digestion maleimide labeling without the serial salt decrease step shows gaps and cracks in the muscle cells at the midbody region. Scale bar indicates 50 µm.

We then switched maleimide labeling in the TREx protocol from before to after digestion and we found that it solved the issue of the cracks. We were no longer able to detect any of the big gaps and cracks (Fig. 7A) that we observed before. Taking a closer look in the brain area (Fig. 7A) at the interface between two tissue types we can clearly see many fine structures in the cell. Based on previous studies[22], it is already known that cracks and distortion in the sample are the result of inadequate digestion. However, since we kept the digestion step unchanged, our results suggest that the pre-digestion maleimide labeling step was the key contributor to the observed cracks and gaps.

Work done by other researchers in Expansion Microscopy on zebrafish[23] has revealed that heterogeneous tissues in the sample exhibit different expansion kinetics. They stressed on how important it was to take measures for these differences. Interestingly, the effect of these cracks could be reduced by implementing a serial decrease of salt concentration during expansion. This slows down the overall sample expansion rate and allows heterogeneous tissue to expand evenly and thus reducing the amount of tissue distortions. Even when the maleimide labeling was done before digestion, we saw improvements on structural integrity by adding this decreased salt concentration step during expansion (Fig. 7B). Cracks and gaps are only observed when these serial steps are omitted (Fig. 7C).

At the start of the project, pre-Incubation was done in the small volume gelation chambers with APS and 4HT. One thing we noticed is that gel polymerization is inhibited by air exposure. This was noticed during preparation of the gel in a vial where closing the vial caused it to harden while keeping it open caused the gel to remain in a fluid state for a longer while. The authors of the TREx protocol in our department determined that a mistake was published in the composition of the monomer solution, and consequently they revised the composition. The percentage of the accelerator TEMED was reduced and so we adapted our gel to this to see how it would perform. Initially we found no major differences in the expanded fish. However, this adaptation did give us a slower reaction which allowed easier pre-incubation of the sample in a larger volume of gel solution. Zebrafish larvae could now be placed in an Eppendorf instead of the chamber. After preincubation the fish could be transferred into the gelation chamber and topped off with fresh solution followed by the rest of the protocol.

Handling the fish & gels

After expanding the zebrafish in gel, we discovered that the gel required handling with caution as it was prone to breaking easily. Especially the thinner gels would also flip over themselves which when moved around in the dish which could cause the gel to tear (Fig. 8A). The fish were found to be transparent after expansion. The overall size and location of the fish inside the gel could be inspected by illuminating the dish containing the gel from beneath with an inverted microscope (Fig. 8A). After localizing the expanded fish, we cut the gel using a knife in the shape of the coverslide or by using a cookie cutter with the same format as the coverslide. The gels were mostly placed on a rectangular coverslide which fit in a custom holder for image acquisition (Fig. 8C). We found that it is best to place the long end of the fish parallel with the long side of the imaging chamber to facilitate image acquisition. Placing it at an angle can create regions with no image, especially during mosaic image acquisition, unnecessarily increasing acquisition times. An alternative was to place the gels on a circular coverslip in an imaging ring since they could be rotated to the desired position.

We experimented as well with different gel sizes and heights to see if there was a difference in expansion factor (Fig. 8B). The parameters can be seen in the *table 1*. Although this experiment was not repeated, we found that overall, the TREx gelation chambers had the highest expansion factor, and that a smaller diameter had a smaller expansion factor as well. Thinner gels also had a lower expansion factor. However, the problem with placing zebrafish in thicker gels is that the fish may end up positioned in the gel in a manner where it does not lie flat on the coverslip, but instead at an angle inside the gel, which creates difficulties for acquiring many features in one Z-section. Furthermore, depending on the imaging setup, the objective working distance can also be insufficient to image the sample if it was positioned higher in the gel. Thinner gels on the other hand experience fewer difficulties in this regard, however, they dry out quicker while imaging (Fig. 8D) so it is important to keep the gel somewhat wet.

The expansion factor of the gels with different heights and sizes were measured with a ruler but in order to get a more accurate estimation of the expansion factor, fluorescent patterned grids on coverslips could be used in combination with TREx. Such a fluorescent grid is being developed in our department, and we briefly tested this (Fig. 8E) and found that it is a straight-forward approach to determine the expansion factor, visualize distortions and to see how the fish is positioned in the gel. Additionally, when you locate a region of interest on a sample, you can record its location found on the grid for efficient navigation back to the specific feature of interest.

Height	diameter		
	4mm	*8mm*	*12mm*
0.25mm	N/A	6.2X	6.4X
0.45mm	4.4X	6.2X	7.1X
0.5mm	4.2X	6.3X	7.1X
0.8mm (TREx)	N/A	N/A	8X

Table 1 | **Expansion factors of different gel sizes & heights.**

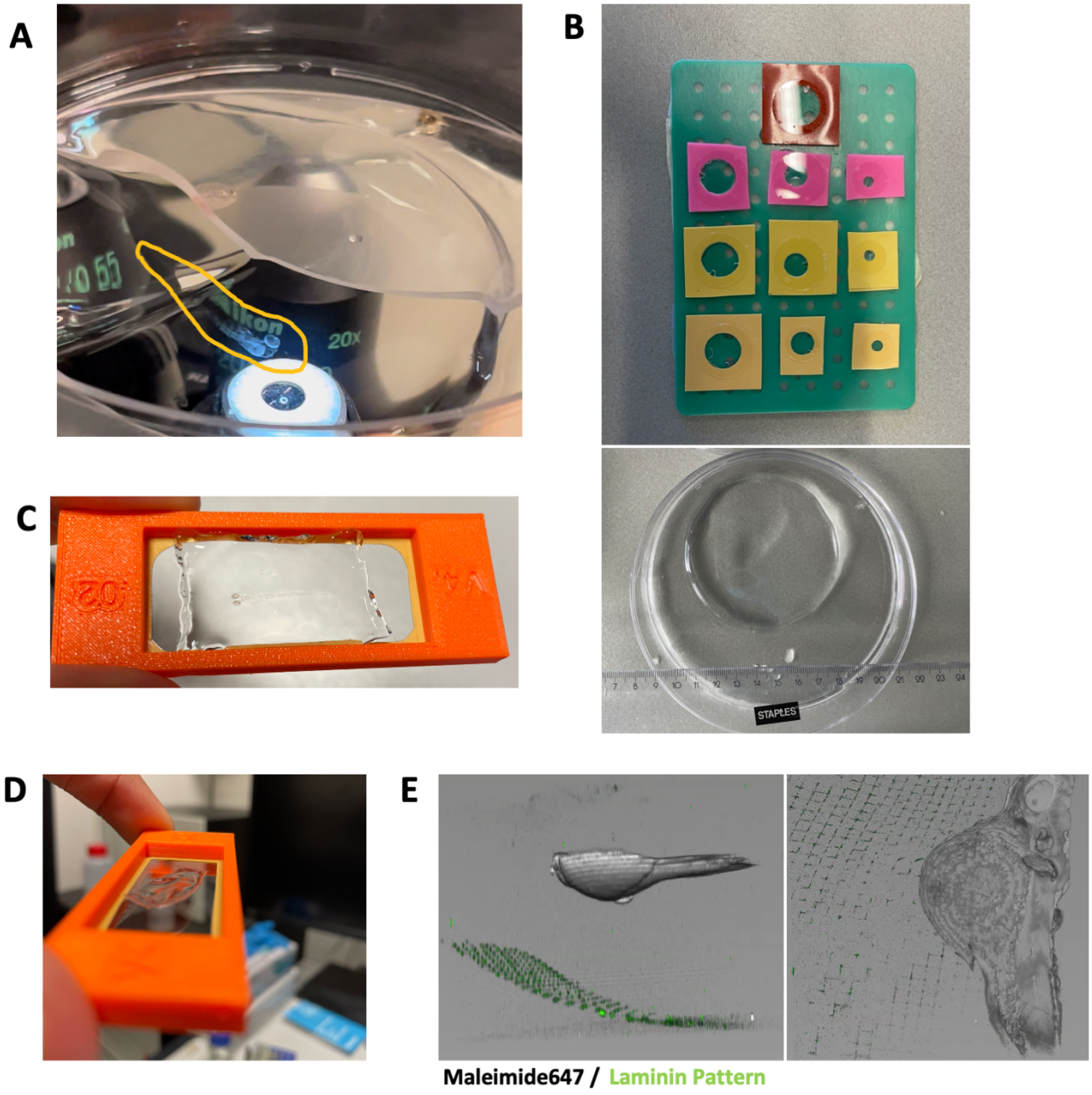

Figure 8 | **Gel handling steps and patterned grids**. **(A)** Fish can be seen by illuminating a dish with gel. This gel also has a tear at the left part showing gel fragility. **(B)** gelation chambers with different heights and diameters can be seen (from table 1) bottom image shows how expansion factors were measured **(C)** Best orientation in coverslip holder for imaging. **(D)** Gel has shrunken considerably after imaging **(E)** Images show pre-expansion zebrafish labeled with total protein Maleimide 647 and the Laminin-594 Fluorescent Patterned grid amplified with 488. distance fish from bottom of gel can be seen, left image shows side view, right image shows top view.

Localizing EVs inside zebrafish

After optimizing the necessary steps of expansion while retaining tissue integrity, we proceeded with detecting and resolving EV structures in zebrafish embryos. From work done previously on this animal model, we knew that EVs accumulate in the CVP area (Fig. 9A), so we focused our imaging efforts there. We performed our optimized TREx protocol on the zebrafish based on all the lessons we learned from the experiments and found that after expansion, a significant increase in resolution was achieved (Fig. 9, B, C and D) compared to the data we obtained before in non-expanded larvae (Fig. 9A). In short, 3-4dpf kdrl:HRAS.mCherry larvae expressing CD63-pHluorin in the YSL were cut in half where pHluorin (a: rabbit anti-GFP-488 antibody) and mCherry (b: Chicken anti-RFP-594 antibody) were fluorescently labeled with antibodies a and b respectively to visualize CD63-pHluorin positive EVs and vasculature after expansion. The fish were labeled using a previously established labeling protocol from our lab and expanded using our now optimized TREx protocol for zebrafish.

Since we were imaging the tail of the zebrafish, we were able to embed the fish in a thinner gel. Zebrafish embryos are much thinner across the tails compared to the midbody and head (Fig. 11), this enabled us to embed the tails in a gel with a smaller height. We used a silicon gelation chamber with a height of 0.25mm, which is smaller than the normal TREx chamber of 0.8mm. Consequently, the fish would occupy more space along the height of the gel, making imaging easier. With this we proceeded to imaging the expanded zebrafish.

This now optimized protocol for the zebrafish resulted in an expansion factor of 4.5. The results also clearly demonstrate that visualization of EV like structures inside the CVP area of the larvae is possible (Fig. 9D). We could now observe with more detail how EVs interact with the vasculature of the zebrafish (Fig. 9, C and D) compared to the observations we had prior to imaging this area without expansion (Fig 9A). Some EVs were found in the blood vessel lumen close to the blood vessel wall, potentially binding to surface proteins while others appeared to be engulfed by it and some appeared to be on the other side of the blood vessel membrane (Fig. 9D). We believe that our findings also revealed some EVs in the process of endocytosis (Fig. 10) characterized by the blood vessel membrane conforming to the shape of the EVs (Fig. 10). Although there was some heterogeneity in EV size, many of them were found to be in the 100-150nm range suggesting that they are indeed exosomes. Perhaps these larger EVs are clusters of single EVs. In conclusion, we were able to show that TREx can indeed be utilized to visualize single EVs *in vivo.*

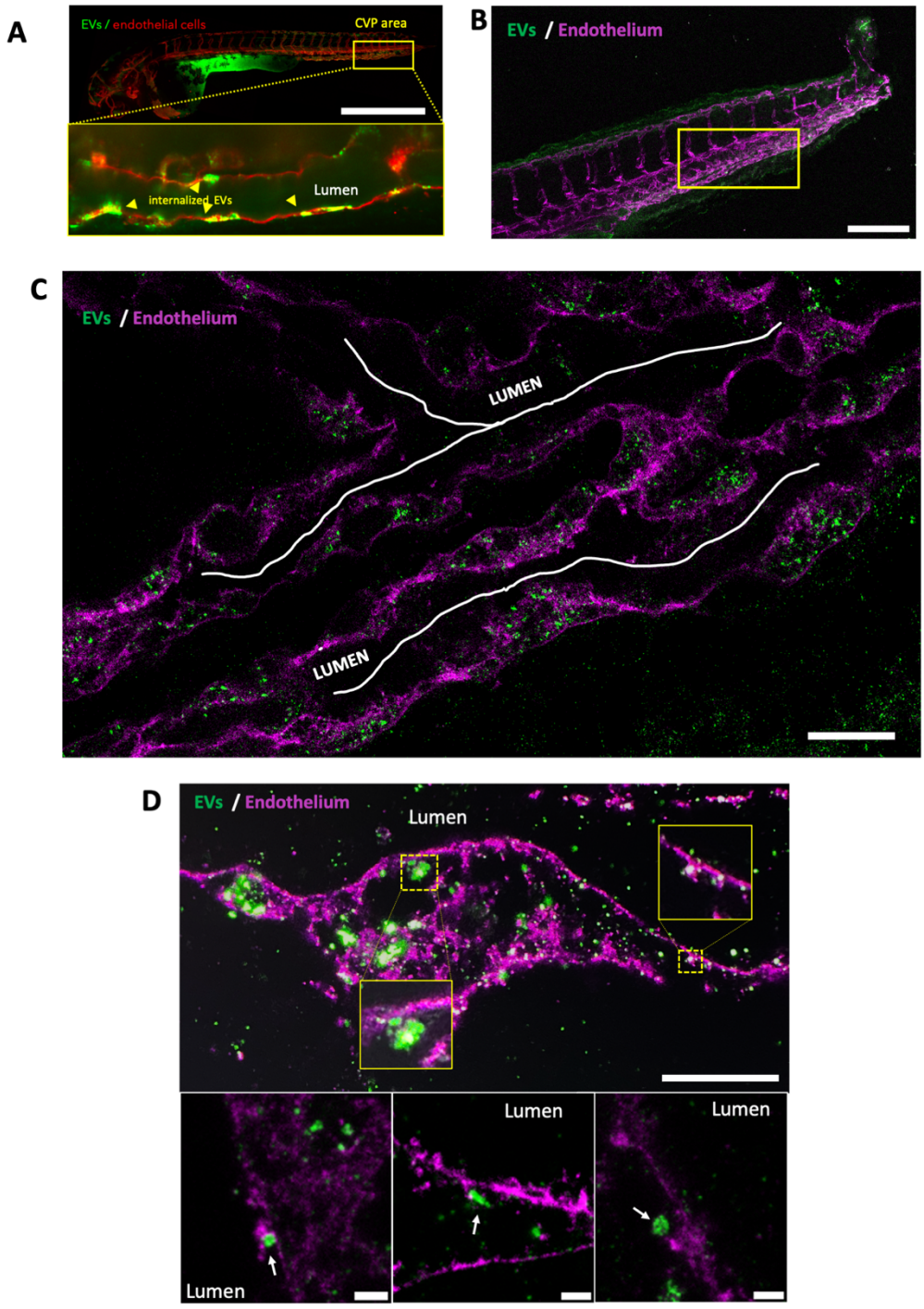

Figure 9 | **EVs *in vivo* at CVP area of zebrafish embryos (A)** Overview of zebrafish CVP area with Vasculature and EVs labeling. The zoomed in portion shows the resolution constraint without expansion. Scale bar indicates 1 mm. **(B)** Expansion of the zebrafish tail. Scale bar indicates 250 µm. Yellow square indicates region **(C)** where we have a much clearer view of the blood vessels and the EVs. Here we can also see the Lumen of the blood vessels. EVs positive for CD63-pHluorin were fluorescently labeled with anti-GFP-488 and the KDRL-mCherry blood vessels were labeled with anti-RFP-594 antibodies. Scale bar indicates 20 µm. **(D)** Top image shows close view of blood vessel membrane in image C. EVs can be seen tethered around the blood vessel wall. Some appear larger than others. Scale bar indicates 5 µm. Bottom images from left to right shows EVs indicated by arrows outside the vessel wall, being engulfed by it and inside the wall tethered to the membrane respectively. Scale bars indicate 1 µm.

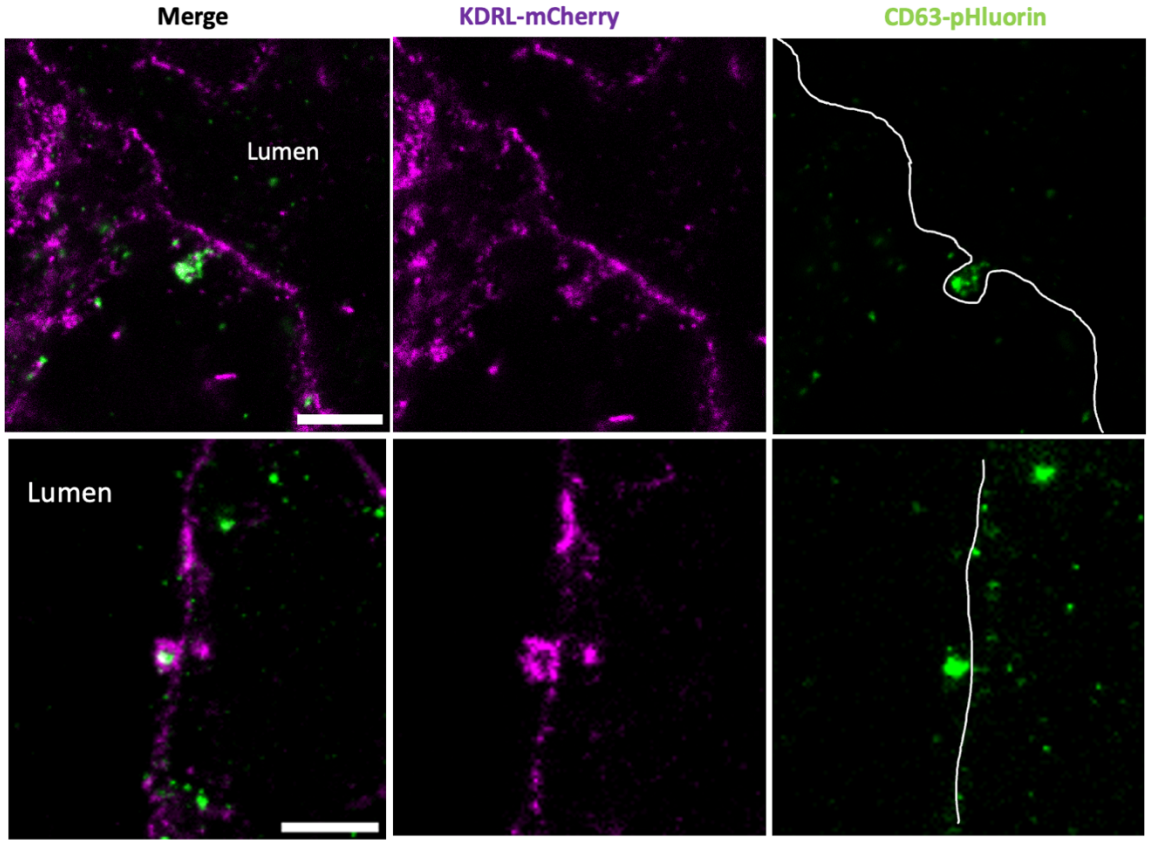

Figure 10 | **Endocytosis of EV at blood vessel membrane.** Here we see examples of how the EV interacts with the blood vessel membrane. Middle images of KDRL-mCherry channel show how the membrane deviates from a straight line in the shape of the EV. Top row shows how EV was likely in the process of endocytosis. Bottom row shows how the EV is completely wrapped by the membrane. This could perhaps be a glimpse of transcytosis since the membrane is wrapped around the EV on the lumen side of the blood vessel. Scale bars indicate 2 μm.

Methods

Cell Culture

Cell lines used were HeLa Wt, U2OS & Vero Wt. All cells were cultured in DMEM medium supplemented with FBS at 37degrees and passaged at ~90% confluency on a weekly basis. Transfection was performed when cells were ~60% confluency. Washing steps were done in Dulbecco's PBS. Cells were trypsinized and split 1:7 for both HeLa and U2OS. Recombinant DNA was transfected into the culture using JetOptimus DNA transfection reagent. Cells prepared for regular microscopy were seeded in 24 well plates on 12mm coverslips. For expansion microscopy cells were seeded in 12 well plates on 18mm coverslips. Cells prepared for fluorescence microscopy were chemically fixated with 2-4% warm PFA, then washed 3x with PBS followed by permeabilization with 0.1% Triton-X 100 and finally blocking in 3% BSA In PBS. Cells were mounted on glass coverslides with 5-8µL of Prolong Gold for 12mm coverslips and 8-11µL for 18mm coverslips.

To study GTPase MVB markers, 150ng of Arl8b GTPases (Constitutively active Arl8b-Q75L-GFP; Dominant negative Arl8b-T34N; Wildtype Arl8b-wt-GFP) was transfected with 350ng of CD63-pHmScarlet in HeLa cells. We had ORP1L variants with RFP and HA tags. We combined 350ng of ORP1L-dORD-HA with endogenously labeled CD63. We used a mouse primary antibody for CD63 at a dilution of 1:100. Except for expansion microscopy, all IF secondary labelings were done at a dilution of 1:1000. For expansion we used secondaries at 1:200 and 1:250. To investigate the ER and MVBs, we transfected 450ng of ORP1L variants combined with endogenous calnexin immunofluorescence labeling. Calnexin was the exception which required a different fixation method of with 4% PFA 0.1% GA and 4% sucrose. We used a rabbit anti-calnexin primary antibody at a dilution of 1:500. In case of VAP-A-HA, we used a 1:1 ratio with ORP1L variants at 250ng and 350ng for a total of 500 or 700ng. For expansion we used the same ratio at 450ng for a total of 900ng of DNA. We used a rat primary antibody for the HA tag at a dilution of 1:200. We first transfected ORP1L-dORD-HA and ORP1L-dORDPHDPHD-HA with anti-Calnexin. However, after seeing the effectivity of VAP-A-HA we switched the ORP1L variants to an RFP tag. We used pCMV-CD63-pHluorin (M153R no kozak) to label endosomes with ORP1L-RFP variants. We tested cross reactivity in HeLa cells before we immunolabeled our transfected plasmids. There was no cross reactivity with anti-RFP-rabbit primary antibody from Rockland and anti-GFP-Chicken primary antibody from Aves Labs.

Zebrafish

All zebrafish fish lines were acquired by F. Verweij. All zebrafish were between 3-6 dpf and were delivered in egg medium EB3 and subsequently anesthetized on ice followed by 4% PFA fixation in a 2mL vial overnight for 24-72h at 4 degrees. The zebrafish lines used for this project were; KDRL-mCherry; Stabilin 1 -/- and Stabilin 2 -/-. The size of the zebrafish was inspected using a ruler and eyepiece on a stereo microscope. For the most part the fish are around 4mm in length and 0.7mm in width at the thickest part. After labeling the fish we chose the ones that had the brightest expression of KDRL and CD63-pHluorin. We could study EVs behavior *in vivo* by injecting CD63-pHluorin in the YSL which are fluorescently expressed and circulate in the bloodstream. Here we also fluorescently labeled the KDRL-mCherry vasculature of the zebrafish.

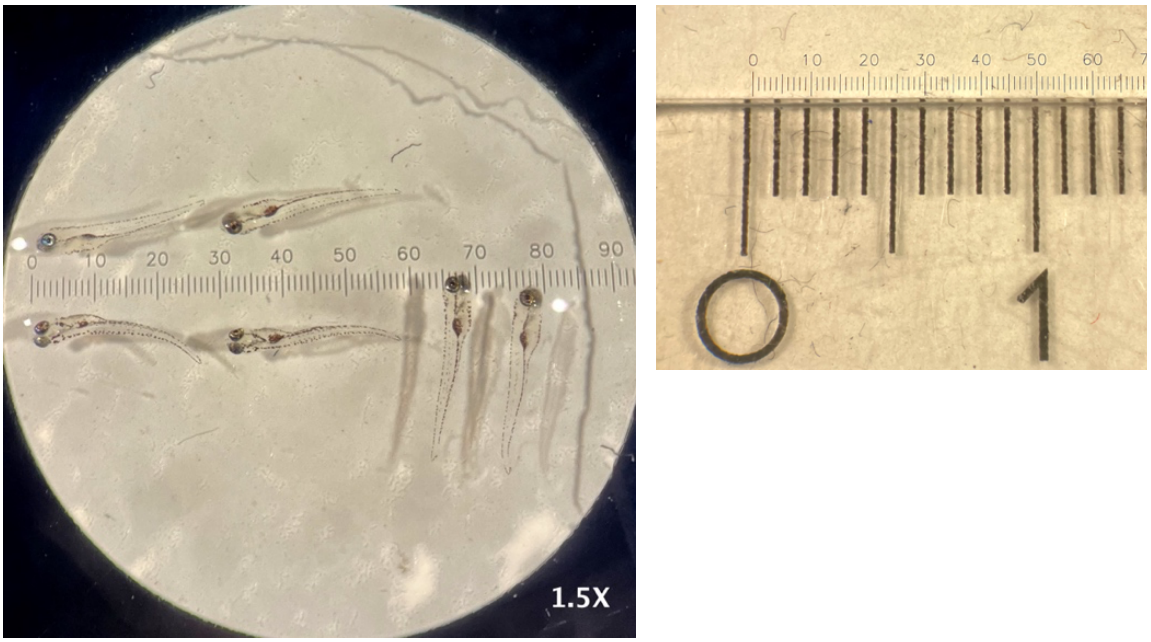

Figure 11 | M**easuring the size of Zebrafish embryos**. Left image shows zebrafish along length and width with the eyepiece ruler markings. Right image shows how this was calibrated to find an average length of 4mm and width of 0.4mm

Hydrogel Recipe

All cells were expanded with a hydrogel recipe based on table below. Halfway during the project, a switch was made to a different monomer solution composition (Table 2). These new gels were more stable and polymerized at a slower rate compared to the previous gel composition.

Chemical	Old gel (µL)	New gel (µL)
Sodium Acrylate	271	271
Acrylamide	360	360
Bisacrylamide	4.5	2.5
PBS (10X)	100	100
MQ	234.5	236.5
TEMED	15 (100% TEMED)	15 (10% TEMED)
APS (10%)	15	15
Total	1000µL	1000

Table 2 | **Monomer solution composition of old and newer gels.**

TREx on cells

TREx protocol was performed according to the protocol by Damstra et al. (See Appendix A). General protein staining with Maleimide647N was added to the protocol. This was done after gelation. Gel was washed twice for 15min in PBS, followed by addition of Maleimide diluted in 2mL PBS. This was done in a 12 well plate for 1.5h at RT. After labeling, the gel was washed in PBS until the excess maleimide was gone. After this the rest of the TREx protocol with digestion and expansion. Expanded gels were placed in special expansion coverslip holders. Here, coverslips were coated with 90 L of Poly-D-lysine to stick gels to coverslip.

Adapted TREx on Zebrafish Embryos

The KDRL-mCherry zebrafish embryos were fluorescently labeled starting with fixation in 4% PFA at 4 degrees overnight or at RT for 2h. Fish could also be stored in 1% PFA for longer periods. After fixation, the embryos were either cut in half or the used as a whole. The embryos were then permeabilized in 0.1% PBST and washed 3x for 10mins. Blocking was done for 1h in blocking solution; 2% BSA, 0.5% Triton X-100 in PBS. The embryos were then incubated in primary antibodies at 4deg overnight in a 500µl vial. We used anti-RFP-rabbit antibodies from Rockland for the zebrafish blood vessels and anti-GFP-Chicken from Aves Labs to label EVs. Both antibodies were used at a 1:250 dilution. This was washed 3X for 10mins in 0.1% PBST followed by secondary antibody incubation. Both secondaries were done at a 1:250 dilution where we used a Rabbit-594 and a Chicken-488 antibody to boost the signal from the sample. The sample was then washed many times with 0.1% PBST. The embryos were then incubated in 10µg/mL Acryloyl-X SE at 4deg overnight. The embryos were then preincubated in gelation solution. Before the switch to the newer gel composition, this was done inside the gelation chamber with 0.015% 4HT and APS at RT. After changing the gel solution composition, fish were placed in a foil covered 24 well plate which was kept open to air exposure to slow down polymerization. This was placed

on ice on a shaker at low speed for 1h. After pre-incubation, the embryos were removed from plate with a brush and placed inside gelation chamber with fresh gelation solution and placed in the 37-degree incubator for 2h. The gelation chambers were made in accordance with the TREx protocol. The chambers could also be sealed with fluorescent patterned coverslips. Here, we acquired coverslips coated with the fluorescent laminin-594 amplified with anti-laminin antibody in 488 from J.B. Passmore (antibody brands unknown). Here, it was important to place the coated coverslip on top to prevent the embryos from moving around too much on the bottom of the chamber when being placed and removing all the protein pattern. The gelated embryos were then placed in digestion buffer with optional DAPI overnight at 37 degrees. The gels were then placed in decalcification solution; 0.3 M EDTA, 1M PBS, 0.1% Triton X-100, pH 8.0, and washed 3 times for 30mins. The final step was a serial salt concentration decrease step. The gel was placed for expansion in 1, 0.8, 0.6, 0.4, 0.2 Molar PBS for 30 mins each time and then finally expanded in 100% MQ. In the decalcification solution and the serial salt decrease we used PBS instead of NaCl. This 100% MQ was refreshed 3-4 times every half hour to an hour and left to expand overnight. The expanded embryos were then cut out of the gel using a special expansion cookie cutter and placed in an imaging holder with the length side parallel with the longest side of the holder (Fig. 8C). Circular coverslips could also be used with imaging rings however these sometimes were a bit harder to place the zebrafish gel without breaking it. The coverslips were first coated with 90µL of poly-D-Lysine just like cells to get the gels to stick. These could then be imaged on the microscope. To determine what expansion factor was obtained, we acquired a mosaic tile image of the length or width of the zebrafish and measured it on the system. This could now be compared with the known average length or width of the zebrafish embryos. We noticed during imaging that the gels can dry out during long periods of imaging. To prevent this, a few drops of MQ can be added on the coverslip in the holder out during imaging. This was especially needed with thin gels (0.25mm) that were expanded.

Microscopes

Most non-expanded cells were imaged on a Nikon 80i microscope with a 100x 1.40NA oil objective. All expanded samples were imaged on the Leica SP8 STED. All expanded cells were imaged with a 63X water objective. To get an overall view of the expanded zebrafish, the 20X air objective was used on the Leica SP8 STED. For more detailed acquisition of zebrafish features in the CVP region of the zebrafish, we used the 63X water objective.

Image Analysis

All images were analyzed and processed with Fiji and light modifications were done to the brightness and contrast. In case images were very noisy some light smoothing was applied. Moreover, some Z-projection was applied on images with about 3-5 slices to get a clearer photo. Renderings in 3D were done with imaging platform Arivis Vision4D.

Discussion

The work in this project showcases how expansion microscopy can be used to visualize EVs *in vivo* and *in vitro*. Here we use TREx microscopy, an improved expansion microscopy protocol capable of achieving a 10-fold expansion factor to observe nanostructures in our specimens that would otherwise not be visible with regular confocal microscopy. We used TREx *in vitro* and found that we can combine the PM bound MVB marker ORP1L with the well-established exosome marker CD63, to label ILVs within MVBs in cells. With this we accomplished our visualization of EVs *in vitro*. To visualize EVs *in vivo*, we adapted and optimized the TREx microscopy protocol on a zebrafish animal model where fluorescent EVs are expressed in the animal, circulate the bloodstream and accumulate in the tail area of the zebrafish. Although we didn't achieve a 10-fold expansion factor, we did achieve an expansion factor of almost 5. The main challenge of optimizing this tool are the many steps along that can all influence each other. Fortunately, with this adapted protocol we could greatly increase the resolution of this area to the point where single EVs could be located. There are many challenges and opportunities when using TREx. We found that the main challenges revolved around properly embedding the zebrafish embryos in the gel and expansion kinetics due to tissue heterogeneity. Here, we discuss key aspects of the project with a more critical perspective and outline recommendations and areas that might be worthwhile to investigate in the future.

In order to visualize EVs *in vitro* we used Arl8b and ORP1L variants as a marker capable of localizing PM bound MVBs. After expressing the MVB markers with CD63, we concluded that ORP1L was a more reliable marker (Fig. 2A; and Fig. 5, A and B) than Arl8b (Fig. 1, A and B). However, there are still some aspects worth discussing around this choice. We made this choice based on ORP1L's more correlative presence near endosomes, and unlike Arl8b, ORP1L did not induce overly enlarged or ring-shaped CD63-positive endosomal compartments (Fig. 2A; Fig. 3, A and C). However, not all Arl8b samples displayed these issues, and it would be interesting to also attempt TREx on this Arl8b marker with CD63. Here we could quantitatively investigate the potential effects of Arl8b (WT/CA) overexpression on late-endosomal maturation in more detail.

Along similar lines, further investigation with TREx is needed to understand the impact the ORP1L variants on MVB maturation. It will also be useful to quantitatively assess if there are significant differences between the size of the MVBs and amount of ILVs of the ORP1L mutants and wildtype variants. We mentioned earlier that ILVs could be more easily visible with the ORP1L-dORDPHDPHD compared to the dORD variant. This is because dORDPHDPHD stimulates MVB progression by allowing minus end MVB transportation to the perinuclear region while dORD inhibits this through stimulation of MCS. From our results (Fig. 5), it seemed that the dORDPHDPHD variant had denser ILV packaging compared to dORD which would support this line of thought. Interestingly, the dORDPHDPHD MVBs also appeared to have a smaller size than dORD, which could be explained by a lack of MCS stimulation, which are known to have a profound impact on MVB maturation[4]. This could be studied in more detail by expressing ORP1L variants (MVBs), VAP-A (ER) and CD63 (ILVs) together. In conclusion, the aforementioned aspects would require more investigation to further be consolidated.

Proper assessment of ILVs requires their clear visualization, however, when we attempted to image ILVs using TREx we found that this was not always the case. A possible explanation for this is that our detergent Triton X-100 was too disruptive. To better resolve the structure of ILVs, we sought to utilize Saponin, a less potent detergent, as a more suitable alternative. However, since saponin did not show any major differences with Triton X-100 (Fig. 4B), this was not further pursued. However, it might very well be that this detergent could have improved the quality of visualization of ILVs packaging as was claimed by fellow EV researcher Maarten Bebelman through verbal communication. Therefore, we recommend that also this approach further be studied.

To get more ultra-structural context of our samples we used Maleimide total protein staining on both single cells and zebrafish tissue (Fig. 4, 5, 6 and 7). This labeling proved quite useful and was bright enough for expansion. Interestingly, there are also other general stainings worth trying such as NHS esters used by other researchers in expansion microscopy[9,23] which also delivered favorable outcomes. Another promising staining is mCLING, used by researchers to study different trafficking organelles. These labeling agents could prove to be useful for zebrafish expansion and investigating MVBs and ILVs.

When it comes to imaging expanded samples, we must consider that not all samples or specimens display the same level of signal intensity. Depending on the labeling protocol, many samples can be extremely dim. This can pose a significant challenge in effectively capturing small details of the sample. Therefore, it is crucial that the users optimize their labeling protocol and also develop a thorough understanding of the imaging setup in order to accurately analyze the samples. Moreover, Expansion microscopy already consists of many steps that need to be executed properly if one wishes to acquire a high-quality image of single cells. Expanding tissue makes this even more complicated as there are even more things to consider, such as incubation times for the thicker tissue, right amount of labeling, differing expansion kinetics and handling of the sample itself to name a few. Fortunately, we were able to image EVs inside zebrafish embryo tissue at the CVP area. Still, we recommend that this experiment be repeated to replicate and improve the results.

One of the key aspects that can be improved is the expansion factor. We achieved an expansion factor of 4.5x which already delivered promising results (Fig. 9 and 10) but in theory we should be able to acquire even more detail with higher levels of expansion. We found that we often got gels that were not 10X expanded, even without containing any specimens (Table 1). This indicates that we might have deviated from the steps somewhere along the protocol. This is most likely an issue of the gel composition. Perhaps we consistently added too much bisacrylamide causing the sample to be overly crosslinked which hinders expansion.

Additionally, it would prove beneficial to add DAPI and/or a general protein staining on the zebrafish for more context in the region of interest when looking for EVs. Moreover, different tactics inspired by other researchers can also be applied, such as multiple rounds of digestion[23]. As we know, proper homogenization of the sample is key to acquiring a good result, especially when working with zebrafish that consists of varying amounts of connective tissue[24]. Although this

would take a lot of time and material, others seem to get results with a lot of detail in their expanded sample using this method. They also do a decalcification step with EDTA which we included in our protocol. It would be useful to analyze the effectivity of this step.

Finally, we briefly attempted fixating the sample in one step using acrylamide/PFA fixation. This technique normally provides a lighter fixation which improves expansion[25]. However, the results we got were not well expanded at all and were therefore not included in this report. This is an avenue that is yet to be explored with expansion of zebrafish embryos. Once we have done this, we could also look at different areas in the fish to see if there are any other places where EVs accumulate. In summary, we expect that future research on all these topics will shed light on all these remaining unknowns.

Conclusion

The study of EVs, nano-size structures released by most cells, requires a high-resolution imaging setup to resolve their ultrastructural features[2]. Expansion Microscopy (ExM) is such a setup capable of providing super resolution microscopy by embedding a sample in a hydrogel and then physically expanding the gel in an isotropic manner which results in magnification[8]. TREx microscopy is an adapted protocol of ExM which increases the expansion factor from 4 to 10-fold resulting in even higher resolution. We used TREx microscopy and found that it is a great tool to visualize EVs *in vitro* on single cells and *in vivo* on zebrafish embryos. The work in this project contributes to the growing knowledge of expansion microscopy but also provides valuable insights and opens new avenues in the growing field of EV research. Especially *in vivo* studies of EVs such as was done in this report can give us a lot more information on EV targets and functions and other intricate cellular biology relationships. We have shown that we can successfully visualize ILVs in MVBs bound for the PM *in vitro* with TREx. Furthermore, we also adapted and optimized the TREx protocol to study EVs in zebrafish embryo tissue. Here we achieved an expansion factor of almost 5-fold. This expansion factor can be improved in the future, however, even with this factor we could already localize single EVs in the zebrafish tissue with much greater detail than we had previously. This only highlights the strong capabilities of this tool. By taking the lessons learned in this project and further building upon them, we can pave the road to a future with exciting EV discoveries. Perhaps in the future, this tool will help us distinguish different EV subpopulations or provide more insights on their biodistribution or targeting mechanisms. As was outlined in the discussion, further aspects of EV investigation remain. In conclusion, it is clear that TREx is extremely useful in the field of EV research and should be further explored.

Bibliography

1. Yáñez-Mó, M. *et al.* Biological properties of extracellular vesicles and their physiological functions. *J. Extracell. Vesicles* **4**, 27066 (2015).
2. Verweij, F. J. *et al.* The power of imaging to understand extracellular vesicle biology in vivo. *Nat. Methods* **18**, 1013–1026 (2021).
3. van Niel, G. *et al.* Challenges and directions in studying cell-cell communication by extracellular vesicles. *Nat. Rev. Mol. Cell Biol.* **23**, 369–382 (2022).
4. Verweij, F. J. *et al.* ER membrane contact sites support endosomal small GTPase conversion for exosome secretion. *J. Cell Biol.* **221**, e202112032 (2022).
5. Chuo, S. T.-Y., Chien, J. C.-Y. & Lai, C. P.-K. Imaging extracellular vesicles: current and emerging methods. *J. Biomed. Sci.* **25**, 91 (2018).
6. Guan, W., Wang, S., Lu, C. & Tang, B. Z. Fluorescence microscopy as an alternative to electron microscopy for microscale dispersion evaluation of organic–inorganic composites. *Nat. Commun.* **7**, 11811 (2016).
7. Asano, S. M. *et al.* Expansion Microscopy: Protocols for Imaging Proteins and RNA in Cells and Tissues. *Curr. Protoc. Cell Biol.* **80**, e56 (2018).
8. Chen, F., Tillberg, P. W. & Boyden, E. S. Optical imaging. Expansion microscopy. *Science* **347**, 543–548 (2015).
9. Damstra, H. G. J. *et al.* Visualizing cellular and tissue ultrastructure using Ten-fold Robust Expansion Microscopy (TREx). *eLife* **11**, e73775 (2022).
10. Valadi, H. *et al.* Exosome-mediated transfer of mRNAs and microRNAs is a novel mechanism of genetic exchange between cells. *Nat. Cell Biol.* **9**, 654–659 (2007).
11. Raposo, G. & Stoorvogel, W. Extracellular vesicles: exosomes, microvesicles, and friends. *J. Cell Biol.* **200**, 373–383 (2013).
12. Al Halawani, A., Mithieux, S. M., Yeo, G. C., Hosseini-Beheshti, E. & Weiss, A. S. Extracellular Vesicles: Interplay with the Extracellular Matrix and Modulated Cell Responses. *Int. J. Mol. Sci.* **23**, 3389 (2022).

13. Yoon, Y. J., Kim, O. Y. & Gho, Y. S. Extracellular vesicles as emerging intercellular communicasomes. *BMB Rep.* **47**, 531–539 (2014).
14. Costa-Silva, B. *et al.* Pancreatic cancer exosomes initiate pre-metastatic niche formation in the liver. *Nat. Cell Biol.* **17**, 816–826 (2015).
15. Pols, M. S. & Klumperman, J. Trafficking and function of the tetraspanin CD63. *Exp. Cell Res.* **315**, 1584–1592 (2009).
16. Johansson, M., Lehto, M., Tanhuanpää, K., Cover, T. L. & Olkkonen, V. M. The Oxysterol-binding Protein Homologue ORP1L Interacts with Rab7 and Alters Functional Properties of Late Endocytic Compartments. *Mol. Biol. Cell* **16**, 5480 (2005).
17. Wijdeven, R. H. *et al.* Cholesterol and ORP1L-mediated ER contact sites control autophagosome transport and fusion with the endocytic pathway. *Nat. Commun.* **7**, 11808 (2016).
18. Verweij, F. J. *et al.* Live Tracking of Inter-organ Communication by Endogenous Exosomes In Vivo. *Dev. Cell* **48**, 573-589.e4 (2019).
19. Hyenne, V. *et al.* Studying the Fate of Tumor Extracellular Vesicles at High Spatiotemporal Resolution Using the Zebrafish Embryo. *Dev. Cell* **48**, 554-572.e7 (2019).
20. Wu, P.-H. *et al.* Lysosomal trafficking mediated by Arl8b and BORC promotes invasion of cancer cells that survive radiation. *Commun. Biol.* **3**, 1–15 (2020).
21. Rocha, N. *et al.* Cholesterol sensor ORP1L contacts the ER protein VAP to control Rab7–RILP–p150Glued and late endosome positioning. *J. Cell Biol.* **185**, 1209–1225 (2009).
22. Klimas, A., Gallagher, B. & Zhao, Y. The Basics of Expansion Microscopy. *Curr. Protoc. Cytom.* **91**, e67 (2019).
23. Sim, J. *et al.* Nanoscale resolution imaging of the whole mouse embryos and larval zebrafish using expansion microscopy. 2021.05.18.443629 Preprint at https://doi.org/10.1101/2021.05.18.443629 (2022).
24. Gaudreau-Lapierre, A., Mulatz, K., Béïque, J.-C. & Trinkle-Mulcahy, L. Expansion microscopy-based imaging of nuclear structures in cultured cells. *STAR Protoc.* **2**, 100630 (2021).
25. M'Saad, O. *et al.* All-optical visualization of specific molecules in the ultrastructural context of brain tissue. 2022.04.04.486901 Preprint at https://doi.org/10.1101/2022.04.04.486901 (2022).